

EGS Collab Project Electrical Resistivity Tomography Characterization and Monitoring

Tim Johnson¹, Chris Strickland¹, Hunter Knox², Jonathan Thomle³, Vince Vermuel³, Craig Ulrich³, Tim Kneafsey³, Doug Blankenship², and the EGS Collab Team.

¹Energy and Environment Directorate, Pacific Northwest National Laboratory, Richland, WA 99352

²Energy Research, Sandia National Laboratory, Albuquerque, NM, 87185, USA

³Earth and Environmental Sciences, Lawrence Berkeley National Laboratory, Berkeley, CA 94720, USA

⁴Energy and Environment Science and Technology Directorate, Idaho National Laboratory, Idaho Falls, ID

Keywords: electrical resistivity tomography, imaging, monitoring, geophysics, Sanford Underground Research Center, hydraulic fracture, flow testing

ABSTRACT

The EGS (Enhanced Geothermal Systems) Collab project is performing stimulation experiments in highly monitored and well-characterized intermediate-scale (~10-20 m) field test beds. The characterization and monitoring system includes an array of electrodes grouted in place within six monitoring wells, with 16 electrodes per well. The electrodes enable characterization of the 3D low-frequency electrical properties of the host rock, and changes in those properties during stimulation and tracer testing using both static and time-lapse Electrical Resistivity Tomography. In this talk we present: 1) ERT array design and installation, 2) baseline (pre-stimulation) imaging results, 3) time-lapse data collected during stimulation operations, and 4) real-time imaging during flow testing. We will also discuss aspects and lessons learned for conducting ERT imaging operations in the presence of high fluid pressure gradients during stimulation and flow operations. Results to date reveal a highly heterogeneous rock fabric, ranging over four orders of magnitude in bulk electrical conductivity. Baseline imaging results reveal the test bed is located within a folded and dipping system of alternating high and low conductivity layers, and are consistent with borehole logs and a discrete fracture map generated from detailed inspection of oriented cores. The raw ERT data show remarkable sensitivity to flow and pressure fluctuations during testing. Time-lapse imaging shows flow initiated in a stimulated fracture enters and is predominantly governed by the natural fracture system. Ultimately the ERT imaging data sets provide critical information for validating and verifying model predictions in preparation for research at DOE's Frontier Observatory for Research in Geothermal Energy (FORGE).

1. INTRODUCTION

The EGS-Collab project is a consortium of U.S. National Laboratories and Universities funded by the U.S. Department of Energy, Geothermal Energy Office, to conduct subsurface fracturing and flow experiments aimed at producing comprehensive characterization and monitoring data sets to test and validate predictive simulators (Keafsey et al., 2019; White et al., 2019). Experiment 1 is located at the 4850 ft. below ground surface drift in the Stanford Underground Research Facility in Lead, South Dakota (Heise, 2015). The test bed consists of 8 boreholes, including one injection and one production well with 9.6 cm diameter, and six monitoring boreholes (Figure 1) of the same diameter drilled into the drift wall. The production and injection wells were drilled parallel to the anticipated minimum stress direction to facilitate hydro-fracturing in planes orthogonal to the well axis (Kneafsey et al. 2015). The injection well was also outfitted with notches to facilitate fracture initiation at locations relatively free from natural fractures as determined by borehole log and core inspection.

The six monitoring boreholes are instrumented with seismic sources and receivers to enable active seismic imaging and passive event detection monitoring during stimulation (Chen 2018a,b). Each well is also instrumented with a continuous distributed temperature fiber for thermal monitoring, and 16 ERT electrodes that enable baseline 3D rock matrix characterization and time-lapse 3D imaging during flow and stimulation events. All instruments were mounted on a rigid conveyance rod, inserted into each borehole, and grouted in place using a low-electrical conductivity grout. For the ERT monitoring array, the primary zone of resolution exists in the region bounded by monitoring boreholes E1-PST, E1-PSB, E1-PDT and E1-PDB (Figure 2).

In this paper we discuss the data collection, inversion results, implications and lessons learned from the ERT data collected to date during pre-stimulation baseline imaging and 3D time-lapse monitoring during hydraulic stimulation and flow testing conducted to date (Knox et al. 2017). Most notably, the ERT baseline inversions reveal valuable information concerning the rock fabric, fracture patterns, and responses observed during stimulation and flow experiments. In addition, raw time-lapse ERT measurements exhibit remarkable sensitivity to flow and pressure conditions, thereby demonstrating the potential of time-lapse ERT imaging to determine when and where current flow is flow altered by changing hydrogeologic conditions. We present several examples and discuss the current status of inverse analysis and interpretation of time-lapse data, ending with a discussion on lessons learned toward improving future ERT array deployments.

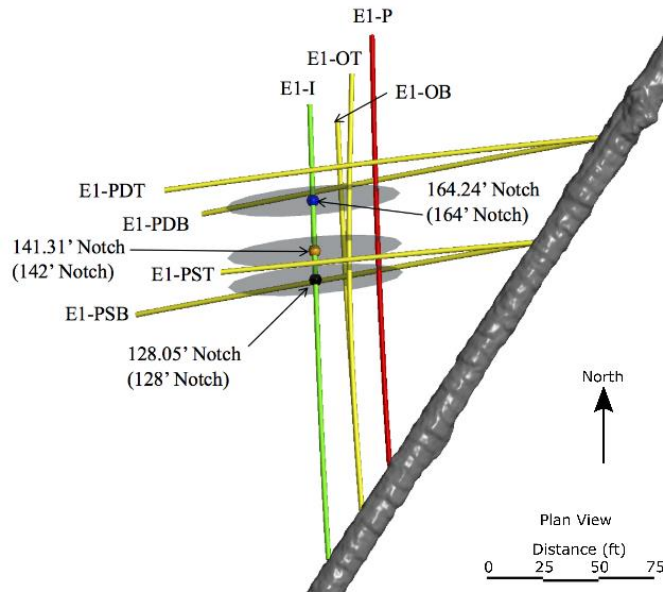


Figure 1. EGS-Collab Experiment 1 test bed. E1-I is the stimulation (or injection) well, E1-P is the production well. The remaining wells are monitoring wells including active and passive seismic sources and sensors, distributed temperature fibers, and electrical resistivity tomography electrodes grouted in place. E1-I was outfitted with notches to aid stimulation at the locations indicated.

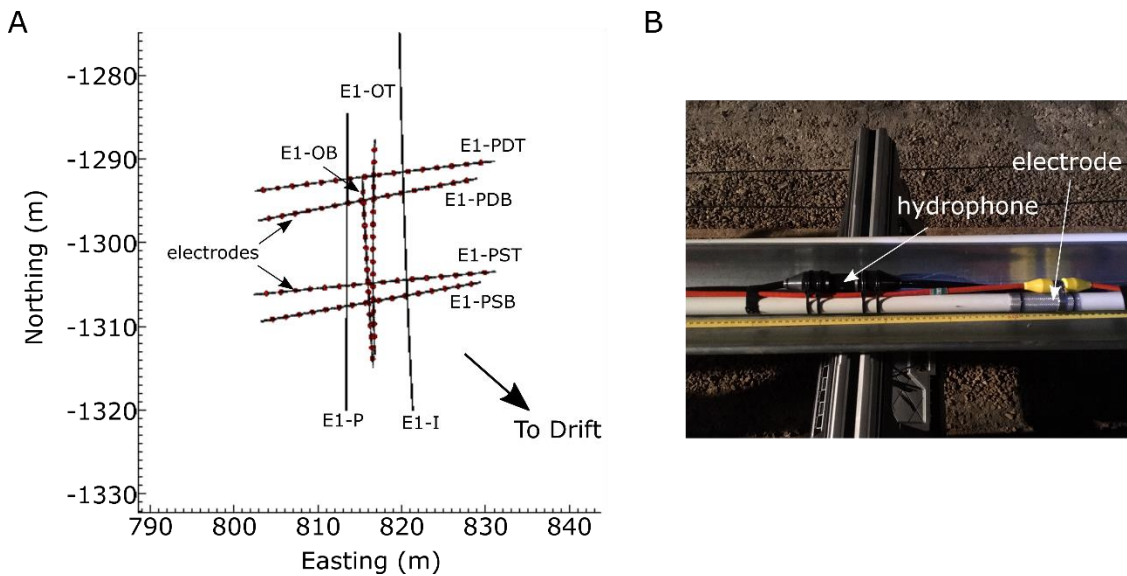


Figure 2. A) Map of electrode locations within monitoring boreholes. B) Image of stainless steel mesh electrode and hydrophone attached to conveyance rod prior to deployment.

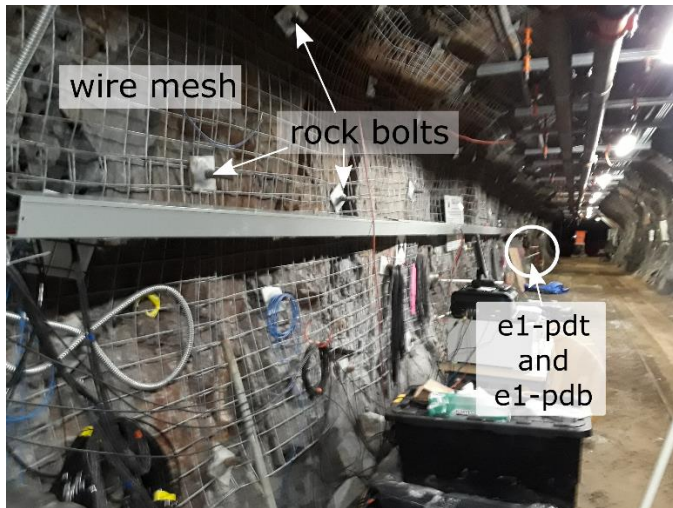
2. REVIEW OF CURRENT FLOW MECHANISMS

A single ERT measurement is conducted by inducing and measuring the current flow between two electrodes (the current electrodes), and measuring the corresponding potential (or voltage) between another two electrodes (the potential electrodes). Many such measurements, strategically chosen to optimization imaging resolution, constitute an ERT survey. The ERT data processing step involves a tomographic inversion, whereby the ERT measurements are used to estimate the bulk electrical conductivity (i.e. the ERT image) of the subsurface that gave rise to the measurements in a survey. In time-lapse ERT, identical ERT surveys are repeated and inverted. The baseline ERT image is subtracted from the time-lapse images to reveal only what has changed over time. Time-lapse imaging is effective for process monitoring when the process of interest modifies subsurface bulk electrical conductivity. For example, transport of electrically conductive fluid can be imaged with time lapse ERT imaging, thereby providing information concerning dominant flow paths within the subsurface.

At ERT current transmission frequencies, current flow within the subsurface is governed by ionic or electronic current flow. Ionic current flow refers to the flow of ions in solution within the pore spaces of the medium in the presence of an electric field. It is dependent upon

the connected porosity (or fracture density) of the host medium, the fluid saturation of the pores (or fractures), the electrical conductivity of the fluid occupying the pore spaces. As bulk conductivity is a measure of the ease at which current flows through a medium, spatial or temporal increases in porosity, fracture density, fracture aperture, fluid conductivity, or saturation will cause a corresponding increase in bulk electrical conductivity and vice versa. Those changes can be imaged by ERT if the corresponding measurements are outside of the electrical noise envelope. Electronic current flow refers to current flow through metallic minerals within the host medium. Electronic current flow is typically orders of magnitude less than ionic current flow in space, and will not change in with time except in the presence of metallic mineral dissolution or precipitation.

3. PRE-STIMULATION BASELINE 3D-ERT IMAGING



imaging of the experiment 1 test bed, as described below.

In this paper we focus ERT efforts associated with stimulation and flow experiments at the 164 ft notch (Kneafsey et al., 2019; Morris et al., 2018) in E1-I (Figure 1). A high-pressure packer system was used to isolate the notch, and pressure was applied in the interval until breakdown. The fracture was then propagated until breakthrough was observed within the production well (see paper by White et. al, this edition). During the experiment, a high pressure packer system was also deployed within the production well, but was not inflated so that the borehole was exposed to atmospheric pressure. Each of the packer systems was connected to surface equipment (valves, pumps, and meters) with a series of 3/8 inch stainless steel tubes, which were in electrical communication with the formation when the boreholes were filled with water. In addition, the 4850 level drift wall and ceiling are supplied with safety netting in the form of metallic wire mesh, fastened to the wall with a series of steel rock bolts (Figure 3). Both the stainless tubing and drift mesh/bolt system were determined to be important considerations for effective ERT

Figure 3. Image of 4850 level drift standing at E1-PST/E1-PSB boreholes and facing northward. Rock bolts and wire mesh form an electrical equipotential surface on the drift face during ERT current transmission.

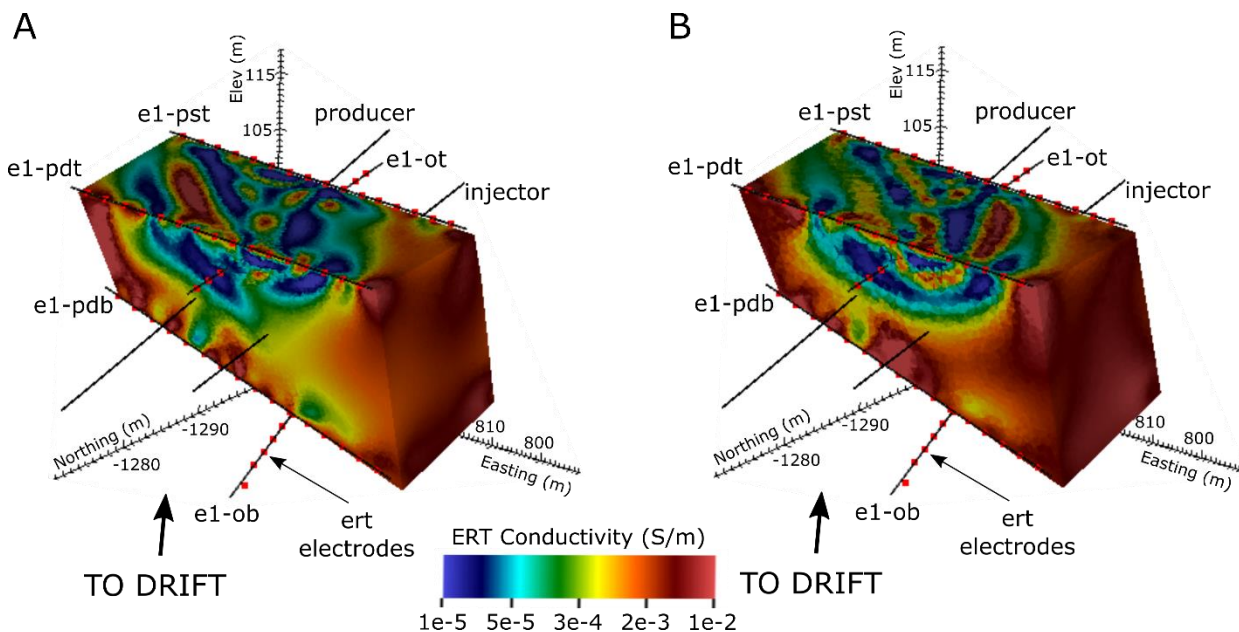


Figure 4. Pre-stimulation baseline ERT image (A) without and (B) with forward modeling of drift mesh and stainless steel packer supply tubing in E1-I and E1-P.

Prior to stimulating at the 164 ft notch, 20 baseline ERT surveys were conducted to establish data noise conditions. Each survey consisted of approximately 1500 dipole-dipole measurements using electrodes in each of the six monitoring boreholes. Using an 8-channel instrument (i.e. 8 potential electrode pairs per current injection), each survey required approximately eight minutes to complete. Time

series of each measurement from the 20 data sets were used to estimate data standard deviations, which establish when the inversion has fit the data to appropriate noise levels. Approximately 50 measurements exhibited excessive noise levels and were removed from the data set.

Ideally, ERT imaging is conducted in regions free from artifact-inducing anthropogenic sources of noise or metallic infrastructure. In this case, both synthetic modeling and data collected with borehole packers deployed at different depths suggested the drift mesh and metal tubing had a significant influence on the ERT data. For practical purposes, the tubing and mesh are essentially infinitely conductive. Consequently, they assume a constant potential and redirect current flow during ERT measurements. Failure to account for influence of the tubing and mesh would force the inversion to estimate the massive conductivity contrast between the formation and the tubing/mesh, ultimately resulting in inversion artifacts and poorly resolved images. A second approach is to explicitly model the influence of the tubing and mesh in the forward modeling step, thereby removing their effects in the inversion. However, standard ERT modelling techniques are unable to maintain stability when simulating the large increase in conductivity between common geologic materials and metal infrastructure (at least 10 orders of magnitude). Instead, we used the approach of Johnson and Wellman (2015), which provides a method of accurately modeling the effects of metallic infrastructure by superimposing multiple partial solutions that are stable with a single unstable solution (see <https://e4d.pnnl.gov>).

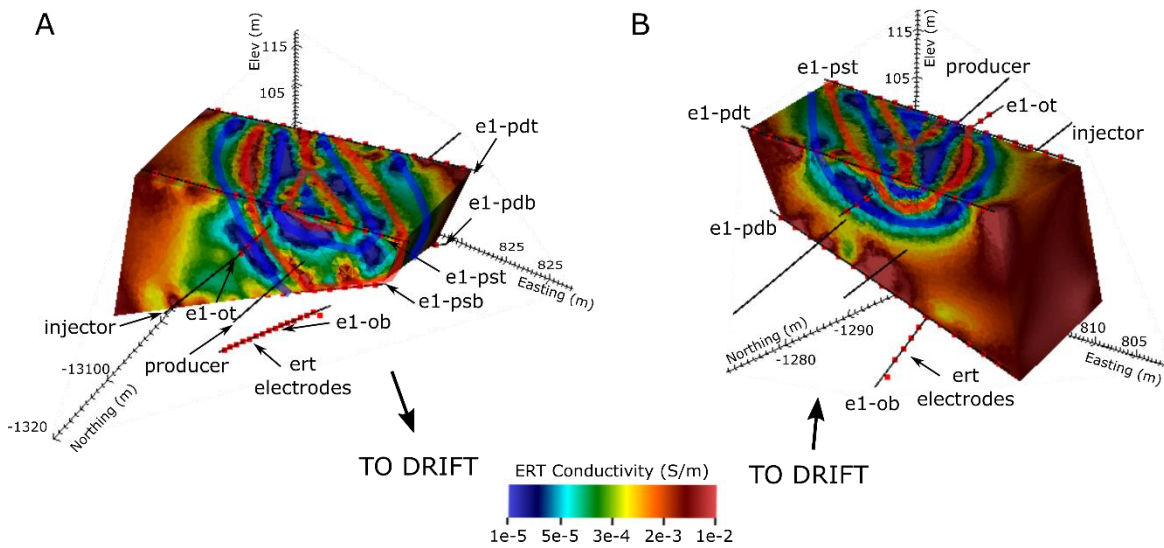


Figure 5. Pre-stimulation ERT images facing (A) away from and (B) toward drift. Transparent lines added to emphasize folded layering of high and low conductivity units revealed by ERT baseline.

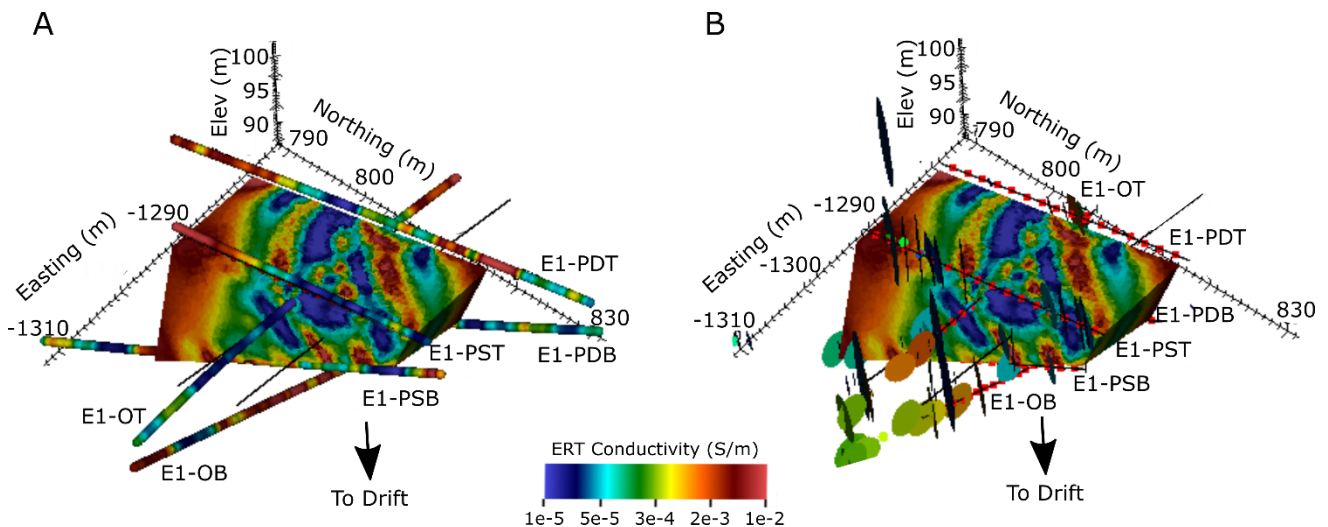


Figure 6. (A) Borehole conductivity logs superimposed on baseline ERT image (Note color scale of logs ranges from the minimum to the maximum conductivity recorded for each log). (B) Fracture locations and orientations derived from inspection of oriented borehole cores.

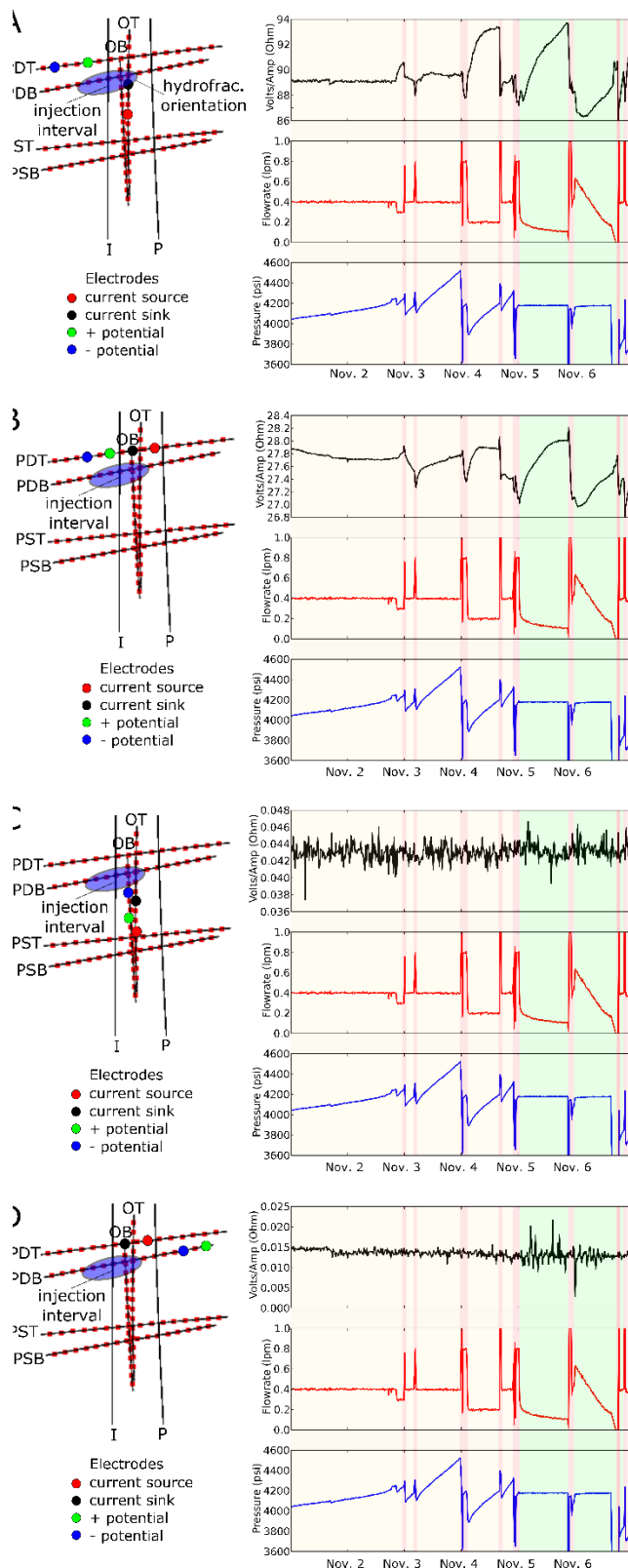


Figure 7. Examples of raw ERT data responses to fracture flow plugging and flushing events. A and B show responses of measurements sensitive to the vicinity of the injection interval. B and D show responses of measurements that are less sensitive to

A comparison of the baseline inversion results without and with explicit forward modeling of the mesh and tubing is shown in Figures 4A and 4B respectively. Figure 4B shows a more coherent rock fabric, and locations of high and low conductivity regions differ between the two inversions. Figure 4B also reveals important information concerning the fabric of the test bed that's further highlighted in Figure 5. Figure 5A and 5B show opposing views of the inversion in figure 4B; 5A is a view from the drift facing the test bed, and 5B is from the far western side of the testbed facing the drift. Each figure is annotated with transparent lines to highlight continuous layers of high (red) and low (blue) conductivity. The baseline image reveals the Experiment 1 testbed is situated within a layered and folded rock fabric with the fold axis dipping to the southeast. The fold is embedded within a more massive and more generally conductive host rock.

The baseline image and structural interpretation described above are validated by direct comparison with borehole conductivity logs and a fracture map constructed through detailed inspection of borehole and core logs shown in Figure 6A and 6B respectively. In figure 6A log-derived borehole conductivity is plotted along each wellbore in color scale. For each wellbore, the color scale spans the range of maximum and minimum conductivity recorded by the log. However, the relative changes in conductivity show excellent agreement with the baseline ERT inversion results. In Figure 6B, natural fractures identified through inspection of oriented borehole cores are shown as circular disks aligned with the strike and dip of each fracture (Roggenthen, 2018). The dominant strike directions are well aligned with the orientation of high and low conductivity layers, suggesting a strong relationship between natural fractures and rock fabric.

3. SENSITIVITY OF ELECTRICAL CONDUCTIVITY TO FRACTURE TRANSMISSIVITY

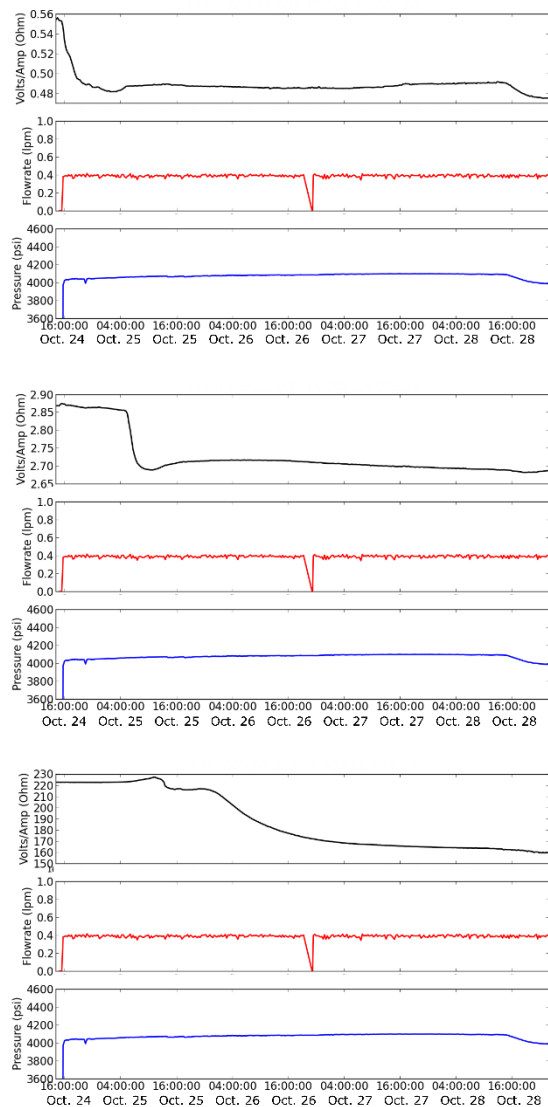
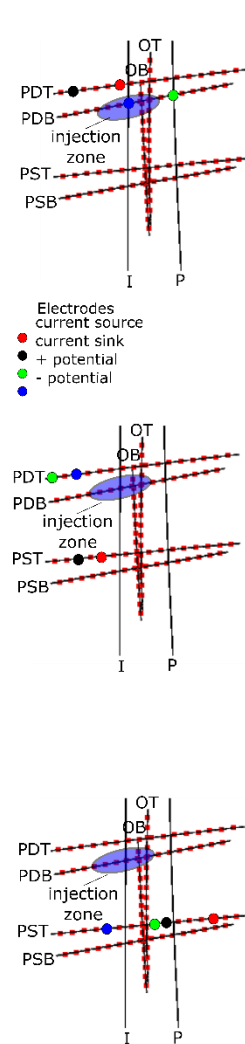
Long term constant flowrate and tracer testing continued through Nov. 1st and Nov. 2nd, 2018. During this period, injection pressures required to maintain a steady flowrate of 400 ml/min began to increase, suggesting a steadily decreasing reduction in fracture transmissivity somewhere within the flow system (see flowrate (red) and injection pressure (blue) lines in Figure 5A through 5D). In an attempt to restore transmissivity, the system was 'flushed' on Nov. 3rd by increasing the flowrate to 800 ml/min for a brief period. After flushing, injection pressure required to maintain 400 ml/min flowrate decreased initially, but began to steadily increase again over time. This prompted a second flushing event with similar results on Nov. 3rd, and twice on Nov. 4th and again on Nov. 5th. After each flushing event the rate of apparent plugging, as indicated by increase injection pressures, appeared to increase. On Nov. 5th the injection was transitioned to constant pressure mode, injected at a pressure of 4,200 p.s.i. Flowrates steadily decreased during constant pressure injection through Nov. 5th, again suggesting plugging or some other mechanism of fracture transmissivity reduction within the system. On Nov. 6th another flushing event was conducted follow by constant pressure injection and corresponding flowrate reduction. Although several possible mechanisms for this unexpected flow behavior have been postulated, the exact mechanism is yet to be identified.

the vicinity of the injection interval. Yellow shading indicates time intervals of constant injection flowrate. Green shading indicates time intervals of constant injection pressure. Red intervals indicate ‘flushing’ intervals of elevated injection pressure and flowrate.

Figures 5A through 5D show time series of selected ERT measurements (black lines) collected during the series of plugging and flushing events described above. The measurement locations were chosen to exemplify data with primary sensitivity to different regions of the test bed. Locations of current injection electrodes and potential measurement electrodes are shown in the diagram to the left of each transfer resistance, flowrate, and pressure plot. Transfer resistance is a measure of the potential recorded across the potential electrodes, normalized by the current injected across the current electrodes, and has units of ohms. An increase in transfer resistance indicates a corresponding increase in the voltage required to induce a unit of current flow, or equivalently an increase in resistance to current flow in the supporting region between the current electrodes. Assuming constant fracture fluid conductivity, and assuming ionic current flow through fracture apertures plays a dominant role in overall current transport, increases in transfer resistance are indicative of corresponding decreases in fracture aperture or increasing in current flowpath tortuosity. This is analogous to the pressure increase required to maintain constant fluid flow within the fracture network under conditions of decreasing fracture aperture or increasing tortuosity.

Figures 5A and 5B show the ERT time-series for measurements with sensitivity to the region surrounding the injection interval where the hydrofracture was initiated. Each response shows remarkable correlation to increasing pressure during constant rate injection, and to decreasing flowrate during constant pressure injection. This suggests that transfer resistance, flow, and pressure are responding to the same mechanism, namely the reduction in fracture transmissivity. In contrast, figures 5D and 5E show ERT measurements with support volumes that are insensitive to the injection interval region. In each case there is no response to decreasing fracture transmissivity. This highlights the utility and sensitivity of ERT measurements for diagnose the timing and location of changes in fracture transmissivity.

4. TIME-LAPSE ERT IMAGING OF FRACTURE-FLOW INDUCED CHANGES IN ELECTRICAL CONDUCTIVITY



After stimulation at the 164 ft notch E1-I and E1-P were opened to atmospheric pressure and the system was allowed to recover for approximately 3 weeks. Subsequently a longer term constant flow test was initiated on October 24th, 2018, including injection and recovery of tracers for residence time measurements. As part of this test, injection water was filtered to reduce fluid electrical conductivity in an attempt to provide an imaging target for time-lapse ERT imaging. At initiation of the flow test, three competing mechanisms were anticipated to influence bulk conductivity with respect to pre-testing conditions. First the injection of relatively low conductivity fluid was expected to decrease bulk conductivity in regions where injected fluid migrated, assuming that the injected fluid maintained its relatively low conductivity (i.e. mineral dissolution did not cause the fluid conductivity to increase). Second, the increase in pressure to open the stimulated fracture and initiate flow causes a corresponding current flow path thereby increasing bulk conductivity. Third after three weeks of rest, the system may have undergone some degree of desaturation. Re-saturation of the system during flow testing caused a corresponding increase in bulk conductivity.

Figure 8. ERT transfer resistance responses for selected measurements with sensitivity near (top), intermediate (middle), and far (bottom) from the injection interval (164 ft notch in well E 1-I). Post stimulation injection testing began at 15:00 hrs on Oct. 24 with flowrate and pressure shown by red and blue lines respectively.

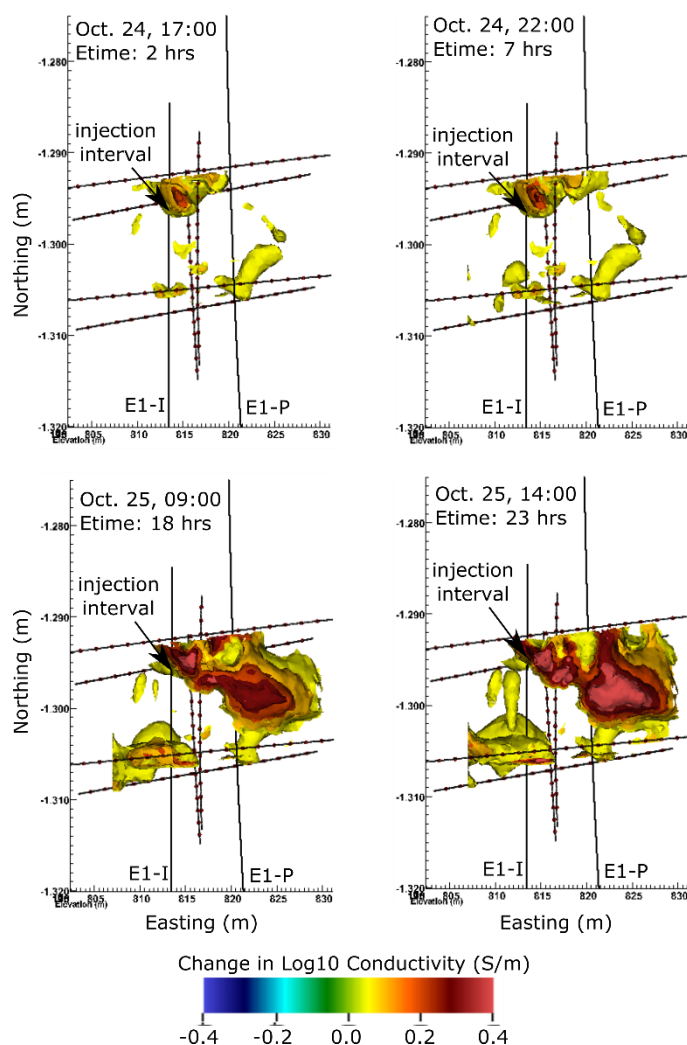


Figure 7. Selections from time-lapse ERT imaging sequence during post-stimulation constant rate flow testing at the 164 ft depth notch (see Figure 1) beginning at 15:00 hrs, Oct. 24, 2018

The baseline image and fracture map shown in Figure 6B suggest the preferred flow pathway corresponds to a fracture zone that intersects the production well E1-P. Time-lapse ERT images collected at 2 and 7 hrs (figure 10) show increased in bulk conductivity that are aligned with the expected plane of the hydrofracture, which is approximately perpendicular to E1-I. Figure 5B suggests that E1-I exits the ERT imaging zone in a relatively massive section beneath the layered and folded fabric. However, the upper extent of the hydrofracture intersects the layers and folds and corresponding system of natural fractures shown in figure 6B. Time lapse images at 18 hrs and 23 hrs show that flow through these natural fractures dominate at later times. Flow within the hydrofracture occurs predominantly near the stimulation well. Once flow is able access the natural fracture system through the stimulated fracture, flow through the natural fracture system becomes dominant.

5. DISCUSSION

Combined with the discrete fracture map in Figure 6B, the static and time-lapse ERT images provide a comprehensive understanding of the interaction between the stimulated and natural fracture systems. Time-lapse ERT images collected at 2 and 7 hrs (figure 10) show increased in bulk conductivity that are aligned with the expected plane of the hydrofracture, which is approximately perpendicular to E1-I. Figure 5B suggests that E1-I exits the ERT imaging zone in a relatively massive section beneath the layered and folded fabric. However, the upper extent of the hydrofracture intersects the layers and folds and corresponding system of natural fractures shown in figure 6B. Time lapse images at 18 hrs and 23 hrs show that flow through these natural fractures dominate at later times. In summary, flow propagates through the stimulated hydrofracture to its intersection with the natural fracture system.

As describe above, static and time-lapse ERT images provide valuable information concerning both the structure and behavior of the testbed during flow testing, and highlights the governing influence of both the stimulated and natural fracture systems. Even so, our capability to adequately fit the ERT data to the observed accuracy was severely limited, meaning that we are unable to extract all of the information in the ERT data through inversion in this case. For example, as shown in figure 7, the ERT monitoring data display remarkable sensitivity to changes in fracture transmissivity and/or permeability. Time-lapse inversion of those data should be able to locate when and where the changes in fracture transmissivity were occurring if the data could be appropriately fit, thereby illuminating the 3D location and

Raw ERT data time series shown in Figure 8 provide insight into which of the mechanisms dominate the bulk conductivity response during the flow and tracer testing. Similar to figure 7, the locations of current injection and potential measurement electrodes are shown to the left of each time series. Measurements are chosen to demonstrate responses of measurements with high (top), intermediate (middle), and low (bottom) sensitivity to the region near the injection zone. The top time-series shows a nearly immediate response to pumping, manifest as a decrease in transfer resistance or equivalently and increase in bulk conductivity with the corresponding measurement volume. This suggests that the either the opening of the hydrofracture or the increase in saturation (or both) at initiation of flow is dominating the response that measurement. The other two time-series also exhibit an increase in bulk conductivity within their respective measurement volumes, except that the responses are delayed as distance from the injection zone increases. These response are consistent with flow moving outward from the injection zone and corresponding increases in saturation and or fracture apertures. There are other time series that show slight increases in transfer resistance, suggesting they are sensing the decrease in injected fluid conductivity (not shown in figure 8). However, the majority of measurements show either no change over time or a decrease in transfer resistance magnitude.

Using the ERT survey collected and inverted on Oct. 24 at 14:00 hrs (i.e. just before the start of the flow test) as baseline, time-lapse ERT inversions were executed to estimate the change in bulk conductivity over time for the first 24 hours of testing. Selected time-lapse inversion results are shown in Figure 10, plotted as iso-surfaces of positive change in conductivity. As suggested by the raw data, the time-lapse images show increases in bulk conductivity originating within the injection zone, and then moving into a preferred flow pathway trending to the southeast.

timing of the plugging phenomena observed from Nov. 2nd through Nov. 7th, within the limits of ERT imaging resolution. The origin of our inability to adequately fit the observed data most likely originates in our inability to model the system with adequate accuracy do to (for example), errors in wellbore positions, extreme heterogeneity in bulk conductivity, variable coupling between the metal packer tubing and the formation, incomplete grouting around the electrode strings, interference from other instrumentation in the same boreholes as the electrodes, high pressure fluid damage to electrodes/cables etc. Many of these sources of errors can be addressed to enable the full potential of ERT characterization and performance monitoring of stimulation and flow operations.

6. SUMMARY

We have summarized the application and status of ERT characterization and monitoring of stimulation and flow operations at the EGS-Collab experiment 1 testbed in the Sanford Underground Research Center mine. Baseline ERT images have revealed important information concerning the 3D structure of the testbed and how that structure is related to the natural fracture system. Time-lapse imaging revealed important information concerning the interaction of stimulated fractures with the natural fracture system in governing flow paths within the testbed. Raw ERT data responses to changes in system performance (i.e. fracture transmissivity) show the rich information available in the raw ERT data, and the corresponding potential of ERT to provide comprehensive 4D monitoring of system flow properties within the limitations of ERT resolution.

ACKNOWLEDGMENTS

Figure 1 was generated using Leapfrog Software. Copyright © Seequent Limited. Leapfrog and all other Seequent Limited product or service names are registered trademarks or trademarks of Seequent Limited. This material was based upon work supported by the U.S. Department of Energy, Office of Energy Efficiency and Renewable Energy (EERE), Office of Technology Development, Geothermal Technologies Office, under Award Number DE-AC05-76RL01830 with PNNL. The United States Government retains, and the publisher, by accepting the article for publication, acknowledges that the United States Government retains a non-exclusive, paid-up, irrevocable, world-wide license to publish or reproduce the published form of this manuscript, or allow others to do so, for United States Government purposes. The research supporting this work took place in whole or in part at the Sanford Underground Research Facility in Lead, South Dakota. The assistance of the Sanford Underground Research Facility and its personnel in providing physical access and general logistical and technical support is acknowledged, with a special recognition to George Vandine for his dedication to this project and safe guidance underground.

REFERENCES

- Chen, Y., L. Huang, J. Ajo-Franklin, T.J. Kneafsey, and E.C. Team (2018a), Toward Real-Time Microearthquake Event Detection and Location in Anisotropic Media Using a Multiscale Approach for EGS Collab Experiments, paper presented at Geothermal Resources Council 2018 Annual Meeting Geothermal Resources Council Transactions, Reno, NV, i:DOI|.
- Chen, Y., L. Huang, and E.C. Team (2018b), Microseismic Moment-Tensor Inversion for the EGS Collab Project: A Synthetic Study, in *PROCEEDINGS, 44th Workshop on Geothermal Reservoir Engineering*, edited, Stanford University, Stanford, California.
- Heise, J. (2015), The Sanford Underground Research Facility at Homestak, *Journal of Physics: Conference Series*, 606(1), 26.
- Kneafsey, T.J., P.F. Dobson, J.B. Ajo-Franklin, C. Valladao, D.A. Blankenship, H.A. Knox, P. Schwering, J.P. Morris, M. Smith, M.D. White, T. Johnson, R. Podgorney, E. Mattson, G. Neupane, W. Roggenthen, T. Doe, and E.C. team (2018b), The EGS Collab Project: Stimulation and Simulation, in *52nd US Rock Mechanics / Geomechanics Symposium held in , USA ,* edited, Seattle, Washington, USA.
- Knox, H., P. Fu, J. Morris, Y. Guglielmi, V. Vermeul, J. Ajo-Franklin, C. Strickland, T. Johnson, P. Cook, C. Herrick, M. Lee, and E.C. Team (2017), Fracture and Flow Designs for the Collab/Sigma-V Project in *GRC Transactions, Vol. 41, 2017* edited.
- Morris, J.P., P. Fu, P. Dobson, J. Ajo-Franklin, T.J. Kneafsey, H. Knox, D. Blankenship, M.D. White, J. Burghardt, T.W. Doe, and E.G.S.C. Team (2018b), Experimental Design for Hydrofracturing and Fluid Flow at the DOE EGS Collab Testbed, in *52nd U.S. Rock Mechanics/Geomechanics Symposium*, edited, p. 11, American Rock Mechanics Association, Seattle, Washington, doi:<https://doi.org>
- Roggenthen, W.M., T.W. Doe, and E.C. team* (2018), Natural Fractures and Their Relationship to the EGS Collab Project in the Underground of the Sanford Underground Research Facility (SURF), in *52nd US Rock Mechanics / Geomechanics Symposium*, edited, American Rock Mechanics Association, Seattle, Washington, USA.